AUTOMATIC IDENTIFICATION OF DOMINANT PHASES AND ANOMALIES IN PANCAM IMAGES OF GUSEV SOILS. M. Parente[1], J. L. Bishop[2] and J. F. Bell III[3]. [1]Stanford University, Packard Engineering Building, 350 Serra Mall, Stanford CA, 94305, cyberey@stanford.edu, [2]SETI Institute / NASA-Ames Research Center, Mountain View, CA 94043. [3]Cornell University, Ithaca, NY 14853.

Introduction: The Mars Exploration Rover (MER) in Gusev Crater has exposed in its tracks an unusual occurrence of a soil high in sulfur and high in phosphorus [1-3] at a site called Paso Robles. Mossbauer (MB) measurements also suggested the presence of ferric sulfate minerals [4]. Ferric sulfates account for about 25–29% of the Paso Robles composition [1]. The sulfate-rich soil is concentrated in the parts exposed by the MER tracks and is typically bright. This bright salty material has been found in other locations such as Arad and Tyrone.

The focus of this work is the interpretation of Panoramic Camera (Pancam) [5] images in the attempt to identify both the dominant and the low abundance phases through their spectral signatures in Paso Robles, Arad and Tyrone soils using automated statistical algorithms as an alternative and/or an aid to expert assessment.

Discussion: Our analysis of Pancam data showed that most scatterplots of the data cloud tend to be tear-shaped or deltoid, radiating away from the so called dark point (greenish area in the right – bottom part of figure 1), the scanner response to a target of zero reflectance in all bands [6] which is close in concept to a virtual endmember as described by [7].

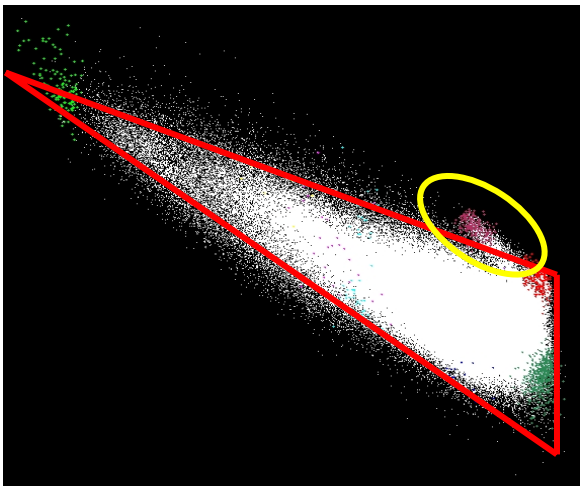

Figure 1: 2-dimensional projection of Tyrone data.

Spectral Mixture Analysis assumes that each mixed pixel on the surface is a linear combination of the spectra of the endmembers. The linear mixing assumption can be retained for intimate mixtures if the reflectance values are converted into single scattering albedo [8]. The shape of the data cloud for the Pancam scenes of Paso Robles, Arad and Tyrone (Tyrone is depicted as an example in figure 1) suggested that linear mixing is a sufficient first order approximation for exploratory analysis of the mineralogy of the sites.

We devised an unmxing algorithm [9] that jointly performs endmember selection and abundance calculation and can operate regardless of ground truth data. When ground truth data on the endmembers is available the algorithm optimizes the calculations by automatically constraining the estimates of the endmembers to vary within certain tolerances. In this particular application we took into account that the dark point must be present as an endmember and that one endmember must be the ubiquitous Martian dust. A more detailed explanation of the unmixing algorithm and an application to remote sensing data can be found in [10].

We validated our unmixing results by comparing the obtained endmembers with the list of all possible endmembers extracted interactively with n-dimensional visualization software embedded in ENVI.

We performed identification of the validated endmembers automatically by comparison with a library of mineral spectra that were convolved with Pancam filter bandpasses. This phase required the calculation of a score measuring spectral similarity and targeted to discriminating between different mineral classes.

The unmixing algorithm is not able to detect low abundance phases because by definition they contribute to the mixture in only a few pixels (e.g. the little purple spur in figure 1 encircled by the yellow ellipse). In order to detect those phases we devised an anomaly detection algorithm [12] that identifies low abundance phases by searching for them in the subspace orthogonal to the mixing subspace [13]. This procedure also allowed us to discriminate outliers and residual artifacts in the images.

The overall algorithm results in an iterative alternation of the unmixing, validation and anomaly detection phases. Details of the procedure will be the focus of an upcoming publication [14].

Paso Robles (Sol400): We concentrated our attention on the area within the red rectangle in fig 2. Sulfate rich soils were exposed in the rover trenches as shown in the abundance map in fig. 3 (in green), resulting from the unmixing. As we can see in fig. 4, this endmember (phase 1) exhibits diagnostic spectral characteristics (e.g., a convex upward feature near 480 nm, a reflectance maximum at ~670 nm and a minimum

near 800-850 nm) that are consistent with a few ferric sulfate minerals, and best fit by ferricopiapite, kornelite, fibroferrite and coquimbite.

Fig 2: Paso Robles area under study.

Coquimbite and kornelite are not identified by MB analyses so we are concentrating our investigation on other minerals [11]. The bright soil spectrum acquired with our technique is consistent with the Paso Robles bright soil reported in [15]. One interesting new mineral match we found for the bright soil spectrum is the phosphate strunzite.

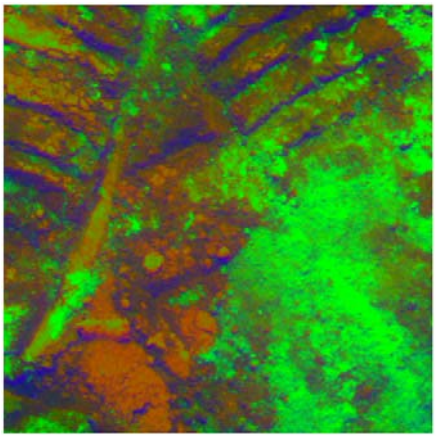

Fig 3: Abundance map for Paso Robles: phase 1 (green), dust (red) and shade (blue).

We also detected a ferric phase (phase 2 in fig 2) that presents a more pronounced band around 800-850 nm and lacks the concave feature at 480 nm. Best matching spectra are again fibroferrite and ferricopiapite.

We also observed a shade endmember and a dust endmember. Our dust spectrum is similar to the typical martian soil spectra observed in previous studies [e.g. 16] and is consistent with spectra of altered volcanic material [e.g. 17].

From the abundance map we remark that the algorithm correctly identifies shade in between the rover marks, dust in the compressed soil and the sulfate in the exposed subsurface soil.

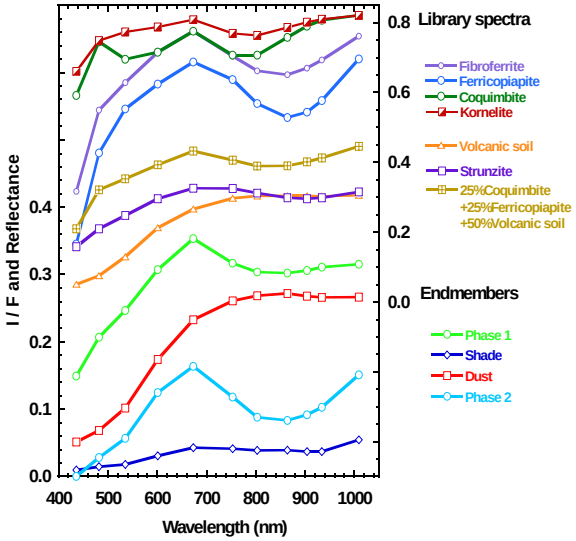

Fig 4: Endmember spectra for Paso Robles sol 400.

Arad (sol 721): Endmember analysis confirmed the expectation that the salty soils exposed by the rover tracks presented sulfate-like signatures consistent with the bright Arad soil in [15]. Figure 5 depicts the area under study while in figure 6 we consider the abundance map of the sulfate with respect to dust and shade. The abundance map positions the sulfate endmember in the exposed soil similarly to Paso Robles.

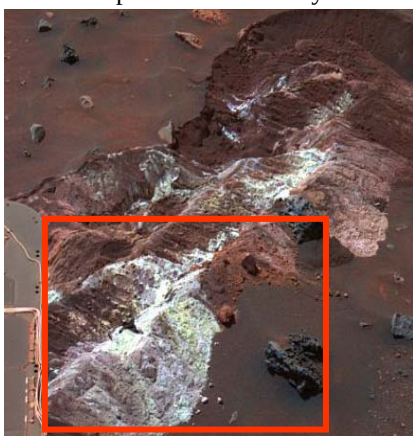

Fig 5: Arad scene under study

Similarly to the features already identified for the sulfate in sol 400, the bright soil 1 endmember at the Arad site (phase 1 in figure 7) showed a reflectance maximum at ~670 nm and a minimum near 800-850 nm but lacking the feature at 480 nm. We argue that the difference with bright soil 1 in Paso Robles is to be ascribed to the fact that the endmember contains a residual dust component mixed with the sulfate species.

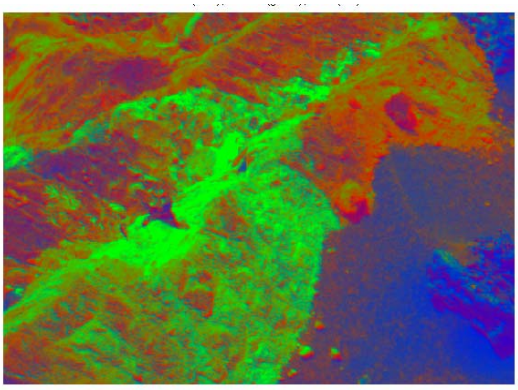

Fig 6: Abundance map for Arad; soil phase (green), dust (red) and shade (blue).

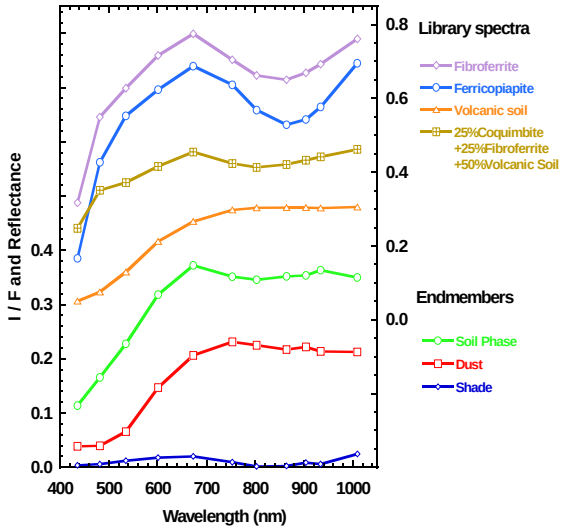

Fig 7: Endmember spectra for Arad sol 721.

We confirmed our hypotheses by mixing the phase 1 spectrum with the dust endmember found in Arad. The resulting aerial mixture in figure 8 seems to have similar characteristics to the sulfate endmember in Sol 721 (soil phase).

Tyrone (sol 790): The exposed trenches created by the rover wheel are depicted in figure 9. In Tyrone soils some peculiar endmember spectra were extracted by our unmixing algorithm along with the prevalent dust, shade and sulfate signatures previously identified in Paso Robles and Arad.

A bright soil spectrum consistent with the "white" Tyrone soil in [15] resulted from the unmixing algorithm (phase 2 in figure 10).

We also identified a phase (Phase 1 in figure 10) consistent with yavapaiite even if present in lower abundance. Figure 11 and 12 represent the abundance maps of bright soil and phase 2 with respect to dust and shade.

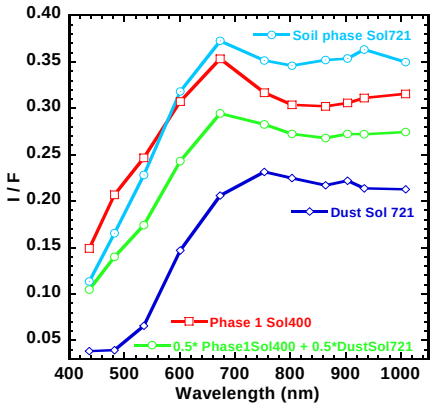

Fig. 8: Comparison of Paso Robles Sol 400 and Arad Sol 721 spectra

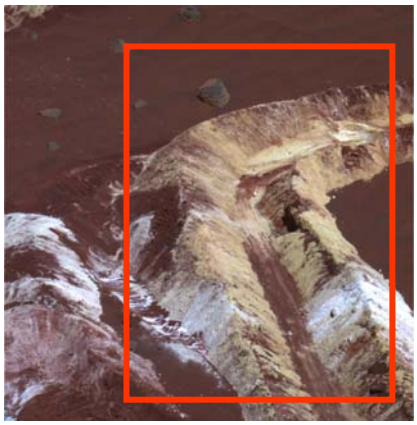

Fig. 9: Tyrone scene under study.

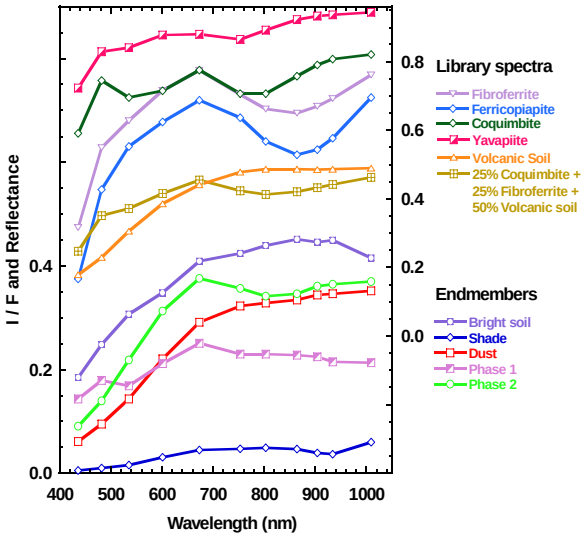

Fig 10: Endmember spectra for sol 790.

It is interesting to point out that the spatial occurrence of phase 2 and bright soil is consistent with the location of similar handpicked spectra in [15], thus

correctly identifying the "yellow" and "white" areas in figure 9.

It is interesting to notice the black areas in figure 11 and 12.They are due to the lack of phase 2 and bright soil respectively because they are not taken into account in the picture.

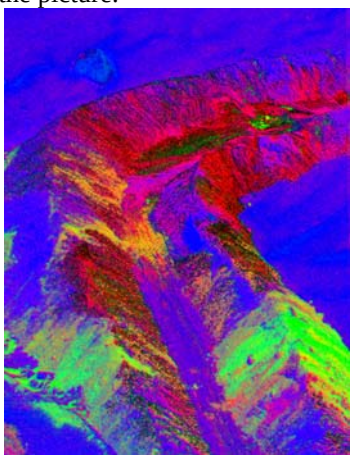

Fig 11: Abundance map for Tyrone; bright soil phase (green), dust (red) and shade (blue).

Low abundance materials: The results of anomaly detection in the Paso Robles, Arad and Tyrone images revealed some interesting results.

From the unmixing analyses on these images we inferred that the dominant sulfate minerals are fibroferrite and/or ferricopiapite based on spectral features at 800-850 nm. Some spectra (Paso Robles phase 1 and Tyrone phase 1) contained an additional feature near 480 nm that is extremely unusual for minerals and is characteristic of coquimbite and kornelite. We were concerned about this identification because the Mössbauer instrument did not identify coquimbite or kornelite. The subsequent anomaly detection procedure confirms that a coquimbite-like spectral signature is present as a low abundance phase as shown in figure 13. Thus, this mineral appears to be present as a minor component that is too low to be detected by Mössbauer, at least in the spots measured so far, but still contributes to the Pancam spectra in isolated regions.

This scenario provides an explanation for the 480 nm hump in some of the endmember spectra extracted from the Paso Robles and Tyrone images.

An additional low abundance spectrum (Sol 400 -2 in figure 13) can be consistent with olivine [15].

Summary: Spectral unmixing has enabled us to map components due to dust, ferric sulfate, and shade in several unusual bright region soils uncovered by the rover tracks in Gusev crater. Possibly a combination of coquimbite or kornelite and ferricopiapite best match the Pancam spectral signature for the sulfate endmember for the Paso Robles sites, fibroferrite best matches the sulfate endmember spectrum for Arad, while for the Tyrone scene together with one sulfate endmember influenced by ferricopiapite we found an endmember with fair correlation to yavapaiite.

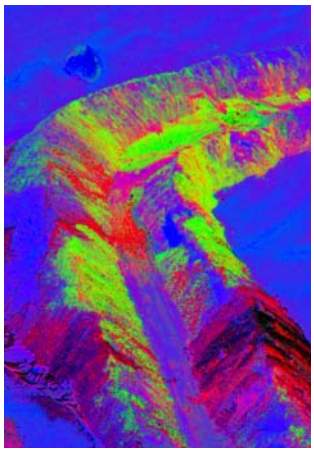

Fig 12: Abundance map for Tyrone; phase 2 (green), dust (red) and shade (blue).

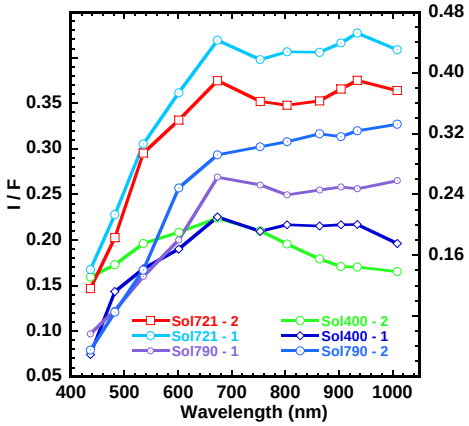

Fig 13: Low abundance materials in Gusev soils.

Anomaly detection permitted the exclusion of outliers and artifacts and revealed interesting additional low abundance phases.

References:

[1] Ming, D. W. et al. (2006) *JGR, 111,* E02S12. [2] Arvidson, R. E. et al. (2006) *JGR, 111,* E02S01. [3] Gellert, R. et al. (2006) *JGR, 111,* E02S05. [4] Morris, R. V., et al. (2006) *JGR,* doi: 10.1029/2005JE002584, in press. [5] Bell, J. F. et al. (2006) *JGR, 111,* E02S03. [6] Craig, M.D. (1994) *IEEE Trans. Geosc. Rem. Sens., 32(3).* [7] Tompkins, S. et al. (1997) *Remote Sens. Environ. 59,* 472-489. [8] Mustard, J.F., and Pieters C.M. (1989) *JGR, 94,* 10376-10390. [9] Keshava N., and Mustard J.F. (2002) *IEEE Sign. Proc. Mag., 02.* [10] Parente, M. ad Bishop J. (2006) *Proc. of SPIE, 6366.* [11] Lane M.D., et al. (2007) *LPSC XXXVIII.* [12] Manolakis, D. et al. (2003*) Lincoln Lab Journal, 14-1.* [13] Ahlberg, J. et al. (2004) *FOI report, R-1526-SE.* [14] Parente, M. et al (2007), *submitted to Icarus.* [15] Johnson J.. et al (2007) *submitted to GRL.*[16] Bell, J.F. et al (1990) *JGR, 95,* 14447-14461. [17] Bishop, J. L. et al (2007) *Clays Clay Miner., 55,* 1-17.